HHS Public Access

Author manuscript

Nat Genet. Author manuscript; available in PMC 2009 September 01.

Published in final edited form as:

Nat Genet. 2009 March ; 41(3): 289–298. doi:10.1038/ng.316.

FGF9 monomer/dimer equilibrium regulates extracellular matrix affinity and tissue diffusion

Masayo Harada[1,2], **Hirotaka Murakami**[3,10], **Akihiko Okawa**[3,10], **Noriaki Okimoto**[4,10], **Shuichi Hiraoka**[1,10], **Taka Nakahara**[5,10], **Ryogo Akasaka**[6,10], **Yo-ichi Shiraishi**[7,10], **Noriyuki Futatsugi**[4], **Yoko Mizutani-Koseki**[1], **Atsushi Kuroiwa**[7], **Mikako Shirouzu**[6], **Shigeyuki Yokoyama**[6,8], **Makoto Taiji**[4], **Sachiko Iseki**[5], **David M. Ornitz**[9], and **Haruhiko Koseki**[1]

[1]RIKEN Research Center for Allergy and Immunology, 1-7-22 Suehiro-cho, Tsurumi-ku, Yokohama, Kanagawa 230-0045, Japan.

[2]Department of Immunology, Graduate School of Medicine, Chiba University, 1-8-1 Inohana Chuo-ku, Chiba 260-8670, Japan.

[3]Department of Orthopaedic Surgery, Graduate School of Medicine, Chiba University, 1-8-1 Inohana Chuo-ku, Chiba 260-8670, Japan.

[4]Computational and Experimental Systems Biology Group, RIKEN Genomic Sciences Center, 1-7-22 Suehiro-cho, Tsurumi-ku, Yokohama, Kanagawa 230-0045, Japan.

[5]Department of Developmental Biology, Graduate School of Dentistry, Tokyo Medical and Dental University, 1-5-45 Yushima, Bunkyo-ku, Tokyo 113-8549, Japan

[6]Protein Research Group, RIKEN Genomic Sciences Center, 1-7-22 Suehiro-cho, Tsurumi-ku, Yokohama, Kanagawa 230-0045, Japan.

[7]Division of Biological Science, Graduate School of Science, Nagoya University, Furo-cho, Chikusa-ku, Nagoya 464-8602, Japan

[8]Department of Biophysics and Biochemistry, Graduate School of Science, The University of Tokyo, 7-3-1 Hongo, Bunkyo-ku, Tokyo 113-0033, Japan

[9]Department of Developmental Biology, Washington University School of Medicine, 660 South Euclid Avenue, St. Louis, MO 63110, USA

Abstract

Correspondence should be addressed to H. K. (koseki@rcai.riken.jp).

[10]These authors contributed equally to this work.

AUTHOR CONTRIBUTION

M. H., D. M. O. and H. K. developed the project and wrote the manuscript. M. H., S. H. and H. K. contributed to the purification of FGF9 proteins, mitogenic assays, analytical gel filtration chromatography, analytical heparin affinity chromatography, surface plasmon resonance analysis, skeletal preparation, histological analyses and *in situ* hybridization of sections, implantation of FGF9 beads in mouse forelimb buds, IP/Western analysis. H. M., A. K. and H. K. contributed to the identification of the *Eks* mutation. N. O., N. F. and M. T. contributed to the MD simulation. T. N. and S. I. contributed to the implantation of FGF9 beads in mouse fetal skulls. R. A., M. S. and S. Y. contributed to the analytical ultracentrifugation. W. S. and A. K. contributed to the retroviral misexpression. Y. M-K. contributed to the *in situ* hybridization of sections.

The spontaneous dominant mouse mutant, Elbow-knee-synostosis (*Eks*), exhibits elbow and knee joint synosotsis, and premature fusion of cranial sutures. Here we identify a missense mutation in the *Fgf9* gene that is responsible for the *Eks* mutation. Through investigation of the pathogenic mechanisms of joint and suture synostosis in *Eks* mice, we identify a key molecular mechanism that regulates FGF9 signaling in developing tissues. We show that the *Eks* mutation prevents homodimerization of the FGF9 protein and that monomeric FGF9 binds to heparin with a lower affinity than dimeric FGF9. These biochemical defects result in increased diffusion of the mutant FGF9 protein ($FGF9^{Eks}$) through developing tissues, leading to ectopic FGF9 signaling and repression of joint and suture development. We propose a mechanism in which the range of FGF9 signaling in developing tissues is limited by its ability to homodimerize and its affinity for extracellular matrix heparan sulfate proteoglycans.

INTRODUCTION

The fibroblast growth factors (FGFs) are widely expressed in developing and adult tissues and have diverse functions in organogenesis, tissue repair, nervous system control, metabolism and physiological homeostasis1. In humans and mice, the 22 FGF ligands are expressed in a spatiotemporally regulated manner and mediate signals through 7 different isoforms of FGF receptors (FGFRs)1. The pharmacologic potential of FGF ligands has been highlighted by identification of gain-of-function mutations in genes encoding *Fgfrs 1–3* in patients with chondrodysplasia and craniosynostosis syndromes2, 3. These human diseases identify essential roles for FGF signaling not only in development but also for homeostasis of bones and joints.

Based on these clinical, genetic and biochemical studies in humans and mice, the coordinated development of bones and joints appears to rely on critical levels of FGFR signaling. This suggests that spatiotemporal constraints on FGF signaling are a prerequisite for appropriate functions *in vivo* and are indeed modulated at several distinct levels. First, there is spatiotemporal restricted expression of FGF ligands. Among the 22 FGF ligands, FGF2, FGF4, FGF7, FGF8, FGF9, FGF10, FGF17 and FGF18 are expressed in the limb bud and developing skeleton4–6. Of these, loss-of-function mutations have demonstrated the involvement of FGF2, FGF9 and FGF18 in chondrogenesis and/or osteogenesis7–10. Induction of chondrodysplastic phenotypes by overexpression of FGF9 in mice also demonstrates its ability to affect chondrogenesis11. Other elements implicated in FGF signaling are the heparan sulfate proteoglycans (HSPGs). Genetic studies in mice and *Drosophila melanogaster* suggest that HSPGs regulate the distribution and receptor binding of FGF ligands12, 13. Finally, structural analyses of FGF9 suggest that it may form homodimers that could affect its ability to signal14, 15. Since FGF9 homodimerization occludes several critical receptor binding sites, an autoinhibitory mechanism may function to modulate FGF9-dependent signal transduction. However, a functional demonstration of this proposed mechanism is lacking.

We have previously reported that a dominant mouse mutant, Elbow-knee-synostosis (*Eks*), exhibits radiohumeral and tibiofemoral synostosis, craniosynostosis (Supplementary Fig. 1), and lung hypoplasia16. In this study, we identify a novel missense mutation, which replaces

Asn143 with Thr in the *Fgf9* gene in *Eks* mutant mice. We designate this mutant allele as $Fgf9^{Eks}$ and show that this mutation prevents homodimerization of FGF9, consequently decreasing the affinity of FGF9 for heparin. As a result, $FGF9^{Eks}$ is more diffusible in developing tissues leading to ectopic FGF9 signaling in the prospective joints and sutures where it functions to repress development. Molecular dynamics (MD) calculations suggest that the reduction in FGF9 affinity for heparin is due to the predominance of the monomeric form rather than to changes in its intrinsic affinity for heparin. We thus propose a mechanism in which the range of FGF9 signaling in developing tissues is limited through regulation of its affinity for HS, which is at least in part controlled by the FGF9 monomer/dimer equilibrium. These observations could have far-reaching implications for the pharmacologic manipulation of FGF signaling under a variety of circumstances and in a wide range of tissues.

RESULTS AND DISCUSSION

Eks is caused by a missense mutation in *Fgf9*

The *Eks* mutation was mapped between the polymorphic markers *D14Mit62* and *D14Mit5* on mouse chromosome 14 (ref. 16). Among 169 genes located in this interval, *Fgf9* seemed a likely candidate for the *Eks* mutation since FGF9 is a ligand for FGFR2c and FGFR3c17 and is expressed in the developing limbs, cranial sutures and developing lung8, 18, 19. Sequence analysis of *Fgf9* cDNA from homozygous *Eks* mice revealed an A to C substitution at position 428, which resulted in the replacement of Asn143 with Thr (Fig. 1a). Intriguingly, the Asn143 residue in FGF9 is highly conserved among most FGF proteins (Fig. 1b) and is predicted to be a critical amino acid residue for homodimerization and receptor binding14, 15.

We used a genetic approach to determine whether the N143T substitution in *Fgf9* was responsible for the *Eks* phenotype. We observed a Mendelian pattern of inheritance of the mutation among 976 offspring of *Eks* heterozygous ($Fgf9^{Eks/+}$) matings, with heterozygous mice exhibiting mild skeletal phenotypes and homozygous $Fgf9^{Eks/Eks}$ littermates exhibiting severe skeletal phenotypes. The *Eks* phenotype and the mutation in *Fgf9* co-segregated in all cases. The absence of recombination between *Eks* and *Fgf9* among nearly 2000 meiotic events provides strong evidence that the *Eks* mutation is allelic with *Fgf9*.

Synostotic phenotypes in $Fgf9^{Eks/Eks}$ are similar to those in gain-of-function *Fgfr* mutants

Eks is a dominant mutation and joint synostosis and premature fusion of sutures have also been reported in mice expressing gain-of-function alleles of *Fgfr1* (ref. 20) and *Fgfr2c* ($Fgfr2^{C342Y}$)21. Furthermore, homozygous *Fgf9* null mutants ($Fgf9^{-/-}$) exhibit rhizomelia but do not show joint or suture synostosis8. Thus we hypothesized that $FGF9^{Eks}$ encodes a gain-of-function mutation. To test this possibility, we first investigated whether there were phenotypic similarities between *Eks* mutants and gain-of-function mutants for *Fgfr1* and $Fgfr2^{C342Y}$. Since initiation of elbow joint development was primarily impaired in *Fgfr1* gain-of-function transgenic mice20, we examined radiohumeral joint development in $Fgf9^{Eks/Eks}$ mice (Fig. 2a–l). *Gdf5* (ref. 22) and *Col2a1* (ref. 23) demarcate the prospective elbow joint and cartilaginous condensation, respectively. *Gdf5* expression in the prospective

joint space was observed as early as E11.5 in *Fgf9*$^{+/+}$ control mice (Fig. 2i), but was completely absent in *Fgf9*$^{Eks/Eks}$ mice (Fig. 2j). Analysis of the prospective cartilage revealed a gap of *Col2a1* expression at the prospective elbow joint in E11.5 wild type embryos (Fig. 2k). The gap of *Col2a1* expression was absent in *Fgf9*$^{Eks/Eks}$ mice (Fig. 2l). In summary, ectopic chondrocyte differentiation in the prospective elbow joint of *Fgf9*$^{Eks/Eks}$ mice appears very similar to that seen in transgenic mice that ectopically express an activated *Fgfr1* kinase domain in the presumptive joint field20.

Premature fusion of coronal sutures in *Fgfr2*^{C342Y} mice results from excess osteogenic differentiation within the coronal suture mesenchyme21. To determine whether *Fgf9*$^{Eks/Eks}$ mice had similar histological features, we examined mineralization and the expression of the early osteoblast differentiation markers *Spp1*24 and *Runx2*25 in the coronal suture. At E15.5, both wild type and *Fgf9*$^{Eks/Eks}$ mice showed similar coronal suture histology (Fig. 2m–t). However, at E16.5 von Kossa staining revealed significantly more overlap of the frontal and parietal bones in *Fgf9*$^{Eks/Eks}$ mice compared to *Fgf9*$^{+/+}$ mice (Fig. 2w, x). *Spp1* expression domains, which demarcate preosteoblasts and osteoblasts, showed wide separation of the frontal and parietal bones in *Fgf9*$^{+/+}$ mice (Fig. 2y), however there was significant overlap in the *Fgf9*$^{Eks/Eks}$ mice (Fig. 2z). *Runx2* is highly expressed in immature osteoblasts at the leading edge of the frontal and parietal bones (Fig. 2a’). In E16.5 *Fgf9*$^{Eks/Eks}$ mice, the intensity of *Runx2* expression in the coronal suture was lower than in *Fgf9*$^{+/+}$ mice (Fig. 2b’), suggesting premature differentiation of the osteoblasts at the presumptive suture. These phenotypes reflect abnormal osteogenic differentiation within the coronal suture mesenchyme and indicate that the defect in suture development occurs before E16.5. Taken together, these observations suggest that the FGF9^{Eks} mutation mediates excess FGFR signals within the prospective joints and sutures, preventing joint formation and promoting the fusion of cranial sutures.

The *Eks* mutation impairs homodimerization of FGF9

The predicted involvement of the Asn143 residue in homodimerization and receptor activation14, 15 suggests that changes in these processes may account for the apparent gain-of-function activity of the FGF9^{Eks} mutant. Homodimerization of FGF9 has been proposed to occlude receptor binding sites and consequently mediate an autoinhibitory mechanism for FGF9 signaling. We thus hypothesized that the *Eks* mutation might impair the autoinhibition. To test this possibility, we compared the degree of homodimerization of wild type (FGF9^{WT}) and FGF9^{Eks} proteins by analytical ultracentrifugation. FGF9^{WT} and FGF9^{Eks} were expressed in *E. coli* and purified by column chromatography (Supplementary Methods and Supplementary Fig. 2).

The molecular mass and association constant of FGF9^{WT} and FGF9^{Eks} were determined by sedimentation equilibrium centrifugation using the purified recombinant proteins (Fig. 3a, b). An estimated average molecular mass of FGF9^{WT} and FGF9^{Eks} was 39,264 and 32,929 Da, respectively, whereas the calculated monomeric molecular mass was 20,090 and 20,077 Da, respectively. These data suggest that FGF9^{WT} primarily exists as a dimer, whereas FGF9^{Eks} exists in a monomer/dimer equilibrium. The calculated association constants of FGF9^{WT} and FGF9^{Eks} were 10.4 μM^{-1} and 0.119 μM^{-1}, respectively. We further measured

the sedimentation coefficient of FGF9^{Eks} by sedimentation velocity centrifugation. The overlay plots of c(s)-sedimentation coefficient distributions show that FGF9^{WT} has a unimodal peak at 3.0 S for a single ideal species, whereas FGF9^{Eks} has bimodal peaks (2.2 S and 3.1 S) for two ideal species (Fig. 3c, d). This observation suggests that FGF9^{WT} is present primarily as a dimer, whereas FGF9^{Eks} exists primarily as a monomer. These interpretations are consistent with the retarded elution of FGF9^{Eks} relative to FGF9^{WT} on a gel filtration column (Fig. 3e). Therefore, FGF9^{Eks} is defective in homodimer formation.

FGF9^{Eks} mediates less potent signaling via all FGFRs except FGFR3c

To examine whether the *Eks* mutaion altered the binding of FGF9 to FGFRs by impairing the autoinhibitory mechanisms, we compared the ability of FGF9^{WT} and FGF9^{Eks} to activate FGFRs by assaying the mitogenic activity of both proteins on BaF3 cells expressing individual FGF receptors17. FGFR-expressing BaF3 cell lines were treated with increasing concentrations of purified recombinant FGF9 in the presence of 1 μg/ml heparin. Compared to FGF9^{WT}, FGF9^{Eks} showed less activity on cells expressing any of the FGFRs except FGFR3c, where FGF9^{Eks} showed equivalent activity (Fig. 4a–g). To test the ability of heparin to enhance FGF9 activity, the BaF3 cell lines were treated with increasing concentrations of heparin in the presence of 0.2 nM FGF9^{WT} or FGF9^{Eks}. FGF9^{Eks} also showed a decreased heparin-dependent mitotic response on all FGFRs except FGFR3c, where FGF9^{Eks} showed higher activity in the presence of high concentrations of heparin (Fig. 4h–n). Since FGF9^{Eks} does not mediate excess signaling via FGFRs, other properties of the mutant protein must be responsible for the phenotype of the *Eks* mice.

The *Eks* mutation lowers FGF9 affinity for heparin

The decreased heparin-dependent mitogenic activity of FGF9^{Eks} suggested that its affinity for heparin may be reduced. Heparin is functionally very similar to HS, which is present in most tissues in the form of HSPGs. HSPGs function to modulate FGFR activation directly, by mediating FGF-FGFR interactions, and indirectly, by binding FGF ligands and regulating their diffusion through the extracellular matrix and thus their access to distant FGFRs1, 12, 13, 26. Since the gain-of-function property of FGF9^{Eks} may not involve direct interaction with the FGFRs, we hypothesized that its decreased affinity for heparin might allow increased diffusion and thus bioavailability in tissues. To address this possibility, we first measured FGF9/heparin affinity by heparin affinity chromatography (Fig. 5a). FGF9^{WT} was eluted from heparin-conjugated agarose with 1.50 M NaCl as a single peak. In contrast, most FGF9^{Eks} was eluted at 1.38 M NaCl and a small fraction eluted at 1.10 M NaCl.

We next measured the kinetic constants for the FGF9^{Eks}/heparin interaction using surface plasmon resonance analysis (Fig. 5b, c and Supplementary Table 1). The resulting sensorgrams were used for kinetic parameter determination by globally fitting the experimental data to a 1:1 interaction model. The association rate constant (k_a) of FGF9^{Eks} was slightly greater than that of FGF9^{WT}, whereas the dissociation rate constant (k_d) of FGF9^{Eks} was 18 fold greater than that of FGF9^{WT}. The dissociation constants (K_D) for FGF9^{WT} and FGF9^{Eks} were 0.71±0.02 nM and 5.24±0.03 nM respectively, representing an 86% decrease in affinity of the FGF9^{Eks} protein for heparin.

Monomeric FGF9 has a lower affinity for heparin than dimeric FGF9

The above studies indicate the FGF9^{Eks} mutation concurrently affects monomer/dimer equilibrium and affinity for heparin/HS. We thus went on to address whether the Asn143Thr mutation directly affects the affinity of FGF9 for heparin versus directly affecting homodimerization and secondarily affecting heparin affinity. However, direct biochemical measurements of the affinity of the two species for heparin are not possible because monomeric and dimeric forms of FGF9 are in equilibrium. We therefore analyzed the configuration of heparin-binding domains in monomeric and dimeric FGF9 using MD simulations and calculated the binding free energy between FGF9 and heparin using the molecular mechanics Poisson-Boltzmann/surface area (MM-PBSA) method. It is well-known that the binding free energies calculated by this method show good qualitative but not quantitative agreement with experimental observations27.

To model the heparin binding affinity of FGF9, we performed MD simulations of 2:2 FGF9^{WT}-heparin and 2:2 FGF9^{Eks}-heparin complexes based on a 2:2:2 FGF2-FGFR1-heparin crystal structure (Protein Data Bank (PDB) ID: 1FQ9)28. The conformations of two heparin oligosaccharides in each complex were influenced by strong electrostatic repulsions, resulting in the exclusion of one heparin oligosaccharide from the complex (data not shown). This analysis suggested that 2:2 FGF9-heparin complexes would be unstable. In contrast, MD simulations of 2:1 FGF9^{WT}-heparin, 2:1 FGF9^{Eks}-heparin, 1:1 FGF9^{WT}-heparin and 1:1 FGF9^{Eks}-heparin complexes suggested that these complexes are stable (Fig. 5d–g). MD simulations of dimeric FGF9-heparin complexes did not show a big difference in heparin-binding free energies for 2:1 FGF9^{WT}-heparin (dimeric FGF9^{WT}-heparin) and 2:1 FGF9^{Eks}-heparin (dimeric FGF9^{Eks}-heparin) complexes (Fig. 5d, e). This is due to the strong interaction between the negatively charged heparin oligosaccharide chain and the array of basic amino acid residues located in the heparin binding site near the groove of the dimer interface in both dimeric complexes. In addition, flexibility of the heparin oligosaccharide chain would help to maintain electrostatic interactions. Similarly, there was little difference in the heparin-binding free energies in 1:1 FGF9^{WT}-heparin (monomeric FGF9^{WT}-heparin) and 1:1 FGF9^{Eks}-heparin (monomeric FGF9^{Eks}-heparin) complexes (Fig. 5f, g). This is also due to heparin oligosaccharide chain flexibility, the strong negative charge of the heparin oligosaccharide and the presence of several basic amino acid residues in the heparin binding site. Therefore, the *Eks* mutation does not appear to influence the heparin binding affinity of either the dimeric or monomeric FGF9-heparin complex. Because the heparin binding free energies for dimeric FGF9 (Fig. 5d, e) were smaller than those for monomeric FGF9-heparin for both FGF9^{WT} and FGF9^{Eks} (Fig. 5f, g), the reduced binding affinity to heparin of the FGF9^{Eks} protein is most likely due to the shift in the monomer/dimer equilibrium towards the monomer. In summary, the *Eks* mutation primarily affects homodimerization of FGF9 and secondarily heparin affinity.

Hyper diffusibility model for joint and suture defects in *Eks* mutants

Heparin/FGF2 interactions have previously been shown to regulate the diffusibility of FGF2 (ref. 26, 29). We hypothesized that the diffusibility of FGF9^{Eks} in tissues would be increased because of its lower affinity for heparin, leading to ectopic localization outside of the normal signaling domain and consequently ectopic activation of FGFRs. However, this model can

only be considered if the following two prerequisites are met; first, *Fgf9* and *Fgfrs* are expressed in the proximity of the prospective elbow and knee joints and coronal sutures and, second, the increased diffusibility of FGF9^{Eks} is dominant over its decreased ability to activate FGFRs.

We first examined the expression of *Fgf9* and *Fgfr1, −2* and *−3* in the forelimb buds in E10.5 and E11.5 mice. *Fgf9* was expressed in migrating myoblasts, both in *Fgf9*$^{+/+}$ and *Fgf9*$^{Eks/Eks}$ mice (Supplementary Fig. 3a, b, i, j). At E10.5, *Fgfr1, −2* and *−3* were expressed diffusely in the limb bud mesenchyme, overlapping the expression domain of *Col2a1* in both *Fgf9*$^{+/+}$ and *Fgf9*$^{Eks/Eks}$ tissues (Supplementary Fig. 3c–h). At E11.5, *Fgfr1* expression was excluded from the cartilaginous condensation, whereas *Fgfr2* and *Fgfr3* expression was observed mainly in this location (Supplementary Fig. 3k–p). Therefore, mesenchymal cells in the prospective elbow joint express *Fgfrs*.

Previous reports showed that *Fgf9* is expressed in the developing frontal and parietal bones, particularly strongly at the rims of the bones18. *Fgfr1, −2* and *−3* are expressed within and around the developing frontal and parietal bone domains30. Thus, the first prerequisite was validated.

FGF9^{Eks} is able to inhibit joint and suture development

To address the second prerequisite for our model, we examined the inhibitory effects of FGF9^{WT} and FGF9^{Eks} on joint development by ectopically expressing them in the chicken limb bud using a replication component retroviral vector (RCAS) transduction. RCAS-*Fgf9*^{WT}, RCAS-*Fgf9*^{Eks}, or empty RCAS virus was used to infect the prospective hindlimb bud region in the lateral plate mesoderm. FGF9^{WT} and FGF9^{Eks} were expressed throughout the hindlimb buds (Fig. 6a, b). Ectopic expression of both *Fgf9*^{WT} and *Fgf9*^{Eks} caused knee joint fusion (Fig. 6c, d, e) whereas no abnormalities were induced by the empty vector (Fig. 6f, g). Therefore FGF9^{Eks} retains inhibitory effects on joint development as well as FGF9^{WT}. It is notable that skeletal defects induced by the expression of FGF9^{WT} were widespread whereas those mediated by FGF9^{Eks} were limited to the prospective joint regions. This is consistent with our finding that FGF9^{Eks} preferentially activates FGFR3c (Fig. 4), which is expressed in the bone anlagen (Supplementary Fig. 3), whereas FGF9^{WT} is expected to activate all of the mesodermally expressed FGFRs.

To examine the inhibitory effects of FGF9^{WT} and FGF9^{Eks} on suture development, FGF9-soaked-AffiGel-Blue beads were implanted in the coronal suture of normal mouse fetal skulls around the initiation stage of the suture defect, at E15, by *ex utero* surgery. We first confirmed that approximately equal amounts of FGF9^{WT} and FGF9^{Eks} were loaded in each AffiGel-Blue bead and that the diffusion rate of FGF9^{WT} and FGF9^{Eks} from the beads was almost identical (Supplementary Fig. 4). The expression of *Spp1*, an early osteoblast differentiation marker upregulated by FGF9, was examined 24 hours after *in utero* bead placement. Grafts of FGF9^{WT} and FGF9^{Eks} beads also promoted ectopic *Spp1* expression at the leading edges of the frontal and parietal bones (Fig. 6h–k). This FGF9-induced ectopic expression of *Spp1* resembled that observed in the *Fgf9*$^{Eks/Eks}$ coronal suture (Fig. 2z). Therefore, ectopic expression of either FGF9^{Eks} or FGF9^{WT} within the suture inhibits suture development.

FGF9^{Eks} is more diffusible than FGF9^{WT} in developing tissues

To examine whether the diffusibility of FGF9^{Eks} in mesenchymal tissue is increased in comparison with FGF9^{WT}, we measured the diffusibility of FGF9^{WT} and FGF9^{Eks} in the skull following bead implantation (Fig. 7a–e). Because FGF9 upregulates *Spp1* expression, we could measure the area of high *Spp1* expression as an indication of the distance over which FGF9 exerts its effects. Implantation of FGF9^{Eks} beads resulted in a larger area of *Spp1* expression (High *Spp1* expression area / Frontal and parietal bone anlagen area = 82.9 ± 7.3%) (± s.e.m.) compared with beads loaded with FGF9^{WT} (50.7 ± 4.4%; P=0.0035) suggesting that the mutant protein diffused more effectively through the developing tissue.

Next, we investigated the diffusibility of FGF9^{Eks} in forelimb buds. FGF9^{WT}- or FGF9^{Eks}-soaked-AffiGel-Blue beads were grafted into the dorsal and central forelimb bud region of *Fgf9*$^{-/-}$ embryos around the initiation stage of the joint defect, at E10.5. FGF9 protein released from the beads into mesenchymal tissue 2 hours after implantation was detected by immunohistochemistry using FGF9 antibodies on sections (Fig. 7f–h). This analysis showed that FGF9^{Eks} permeated through the limb bud mesenchyme to a greater extent (Relative disffusion area = 138 ± 12%) (± s.e.m.) than FGF9^{WT} (100 ± 14%; P=0.043) supporting the hypothesis that FGF9^{Eks} is more diffusible than FGF9^{WT}.

Ectopic FGF signaling in the prospective elbow joint of *Fgf9*$^{Eks/Eks}$ mice

To examine whether diffusion of endogenous FGF9^{Eks} is increased in comparison to FGF9^{WT}, we determined the level of activation of FGFRs in the prospective elbow joint of *Fgf9*$^{Eks/Eks}$ mice. As a readout for FGFR signaling, we examined the expression of *Etv4* and *Etv5*, both of which are known to be transcriptionally activated by FGF signaling, in the forelimb buds31. In wild type E10.5 limbs, we did not observe the intensive expression of *Etv4* or *Etv5* within the region undergoing cartilaginous condensation demarcated by *Col2a1* expression (Fig. 7m, o). However, in E10.5 *Fgf9*$^{Eks/Eks}$ limbs, we found ectopic expression of both *Etv4* and *Etv5* in the cartilaginous condensation (Fig. 7n, p). At E11.5, *Etv4* and *Etv5* were expressed in the myoblasts and cells surrounding the cartilaginous condensation in wild type mice (Fig. 7u, w), whereas in *Fgf9*$^{Eks/Eks}$ mice, we observed clear expression of *Etv4* and *Etv5* in the cartilaginous condensation including the prospective elbow joint position (Fig. 7v, x). These results demonstrate ectopic FGF signaling in the prospective elbow joint in *Fgf9*$^{Eks/Eks}$ mice. Since the ectopic expression domain of *Etv4* and *Etv5* in *Fgf9*$^{Eks/Eks}$ mice was not consistent with the *Fgf9* expression domain (Supplementary Fig. 3a, b, i, j), this outcome is likely due to increased diffusion of FGF9^{Eks} protein over a larger area than FGF9^{WT}.

From these results, we propose a mechanism of elbow joint synostosis in *Fgf9*$^{Eks/Eks}$ mice in which FGF9^{Eks} produced by myoblasts diffuses beyond its normal range and ectopically activates FGFRs in the prospective elbow joint, preventing joint formation (Fig. 7y). Similarly, FGF9^{Eks} produced at the rims of the frontal and parietal bones diffuses beyond its normal area and ectopically activates FGFRs in the coronal suture mesenchyme, promoting the fusion of coronal sutures (Fig. 7z).

Rescue of synostotic phenotypes in *Eks* heterozygous mice by expression of FGF9^{WT}

A prediction of our model is that the severity of synostotic phenotypes will correlate with a shift in the equilibrium of FGF9 from dimer toward monomer. By MD simulations, we estimated that FGF9^{WT} homodimer, FGF9$^{WT/Eks}$ heterodimer and FGF9^{Eks} homodimer have 10, 8, 6 inter-monomer hydrogen bonds, respectively (Fig. 8a–c and Supplementary Table 2). Based on these results, the calculated binding free energy of the FGF9$^{WT/Eks}$ heterodimer was between those of the FGF9^{WT} and FGF9^{Eks} homodimers (Fig. 8a–c). FGF9$^{WT/Eks}$ heterodimers are suggested to be more stable than FGF9^{Eks} homodimers. If our model is correct, FGF9^{WT} should interfere with FGF9^{Eks} action by forming FGF9$^{WT/Eks}$ heterodimers. In other words, skeletal phenotypes due to the *Eks* mutation should be alleviated by the expression of FGF9^{WT}.

We first sought experimental evidence that the FGF9$^{WT/Eks}$ heterodimer was substantially more stable than the FGF9^{Eks} homodimer. We addressed this issue by immunoprecipitation (IP)/Western analysis after tagging FGF9^{WT} and FGF9^{Eks} with FLAG- or Myc-peptides. FLAG-FGF9^{WT} or -FGF9^{Eks} were over-expressed together with Myc-FGF9^{WT} or -FGF9^{Eks} in COS7 cells and the culture supernatants were subjected to the IP/Western analysis (Fig. 8d). We readily detected FLAG-FGF9^{WT}/Myc-FGF9^{WT} dimers. FLAG-FGF9^{Eks}/Myc-FGF9^{WT} dimers were detected at lower level, however, FLAG-FGF9^{Eks}/Myc-FGF9^{Eks} dimers did not form under these conditions. These data suggest that FGF9^{WT} and FGF9^{Eks} can form heterodimers that are more stable than FGF9^{Eks} homodimers.

We finally examined whether the elbow synostosis caused by FGF9^{Eks} could be alleviated by the expression of FGF9^{WT}. We thus compared the severity of elbow synostosis in *Fgf9*$^{Eks/+}$ and compound heterozygous mutants (*Fgf9*$^{Eks/-}$) relative to that of *Fgf9*$^{+/-}$ and *Fgf9*$^{Eks/Eks}$ mice. Elbow joint formation was not affected in *Fgf9*$^{+/-}$ mice (Fig. 8e), whereas elbow synostosis in *Fgf9*$^{Eks/Eks}$ mice involved both cartilaginous and bony components (Fig. 8h). In contrast, the synostosis in *Fgf9*$^{Eks/+}$ mice was limited to the cartilaginous component (Fig. 8f), while the involvement of the bony component in *Fgf9*$^{Eks/-}$ mice was similar to that of *Fgf9*$^{Eks/Eks}$ mice (Fig. 8g, h). Therefore, elbow synostosis in *Fgf9*$^{Eks/-}$ is more severe than in *Fgf9*$^{Eks/+}$. These findings strongly support our model that the monomer/dimer status of FGF9 influences its affinity for heparin/HS and, consequently, its distribution in developing tissues.

Conclusions and biological implications of FGF9 homodimerization

In the present study, we identified a missense mutation in the *Fgf9* gene that is responsible for the *Eks* mutant phenotype, which includes elbow and knee joint synostosis, and craniosynostosis. We further demonstrate that the Asn143Thr mutation in FGF9 favors formation of the monomeric form of FGF9, which binds to heparin with a lower affinity than dimeric FGF9. The decreased affinity for heparin/HS leads to increased diffusion of the mutant protein in developing tissues, resulting in ectopic FGF9 signaling. We propose that regulation of the monomer/dimer equilibrium of FGF9, and potentially of other FGFs, and its affinity for heparin/HS is a mechanism that functions to shape FGF9 concentration gradients in developing tissues. We further propose that these biochemical properties of FGF9 restrict its signaling activity to limited skeletal domains. Data presented here and in

previous studies indicate that low FGF signaling in the presumptive joint space is necessary for the formation of the joint space and maintenance of an open suture20, 21. Common usage of receptor binding and homodimerization sites of FGF9 could be at least in part instrumental for local modulation of FGF9 signaling activity.

Homodimerization is suggested to be a common feature of the FGF9/16/20 subfamily32 and of FGF2 (ref. 33, 34). It is not known to what extent homodimerization affects the activity of other FGFs. The discovery that a mutation in *Fgf9* can affect homodimerization, affinity for heparin/HS, and biological activity suggests that pharmacological agents that affect FGF homodimerization could be useful tools to modulate its activity.

METHODS

Detection of a mutation in the *Fgf9* gene

To identify the mutation responsible for the *Eks* mutant phenotype, we surveyed the cDNA sequence of *Fgf9* from normal (+/+), heterozygous (*Eks*/+) and homozygous (*Eks/Eks*) mice through reverse transcription-PCR (RT-PCR) and direct sequencing of RT-PCR products.

For genotyping of the *Eks* allele, genomic DNA spanning the *Eks* mutation was amplified by PCR using specific primers (Supplementary Table 3). PCR products were digested with the diagnostic *BsrI* restriction enzyme. Wild type mice show two bands of 147 bp and 42 bp, whereas the *Eks* allele shows one band of 189 bp (Supplementary Fig. 5).

Skeletal and histological preparations

Bones and cartilage of E17.5 fetuses were stained with Alizarin red and Alcian blue as previously described35. For histological preparations, tissues were fixed in 4% paraformaldehyde, embedded in paraffin, sectioned at 5 μm, and stained with hematoxylin and eosin and von Kossa.

In situ hybridization

In situ hybridization of paraffin sections was performed as previously described36, using radiolabeled antisense RNA for *Gdf5* (MGI: 95688), *Col2a1* (MGI: 88452), *Spp1* (MGI: 98389), *Runx2* (MGI: 99829), *Fgf9* (MGI: 104723), *Fgfr1* (MGI: 95522), *Fgfr2* (MGI: 95523), *Fgfr3* (MGI: 95524), *Etv4* (MGI: 99423) and *Etv5* (MGI: 1096867). *In situ* hybridization after beads implantation in fetal skulls was performed as previously described24.

FGF9^{WT} and FGF9^{Eks} expression and purification

FGF9^{WT} and FGF9^{Eks} expression and purification were performed as described in Supplementary Methods.

Analytical ultracentrifugation

All analytical ultracentrifuge experiments were performed on a Beckman Coulter XL-I analytical ultracentrifuge. The samples were diluted in 25 mM ammonium acetate buffer (pH 5.5) containing 120 mM NaCl. The partial specific volumes were estimated as 0.7317

mL/g ($FGF9^{WT}$) or 0.7322 mL/g ($FGF9^{Eks}$) by SEDNTERP software. All experiments were performed at 20°C and the absorbance wavelength was 280 nm. Sedimentation equilibrium experiments were carried out with six channel centerpieces, with loading concentrations of 0.8, 0.4 and 0.2 mg/ml. Data were obtained at 12, 14 and 16 k rpm for $FGF9^{WT}$ or at 14, 16 and 18 k rpm for $FGF9^{Eks}$. A total equilibration time of 16 hours was used for each speed with scans taken at 12, 14 and 16 hours. The sedimentation equilibrium data were analyzed using the Beckman XL-A/XL-I Data Analysis software. All nine data sets (three speeds, three concentrations) were fitted together by "Self Association Model" calculation. Sedimentation velocity experiments were carried out with double sector centerpieces. Protein concentrations were 0.4, 0.3 or 0.2 mg/ml. The absorbance data were scanned 100 times every five minutes at 40 k rpm. The measurements data were analyzed by SEDFIT software.

Analytical gel filtration chromatography

Purified $FGF9^{WT}$ and $FGF9^{Eks}$ (100 μl of 2 mg/ml) were loaded onto a Superdex75 10/300 GL column (GE healthcare) equilibrated with a 25 mM ammonium acetate buffer (pH 5.5) containing 120 mM NaCl. The samples were eluted with the same buffer.

Mitogenic assays

The ability of $FGF9^{WT}$ and $FGF9^{Eks}$ to transduce signals via FGFRs was analyzed by a mitogenic assay using BaF3 cells expressing specific FGFRs as described previously17. 5,000 cells were plated per well in a 96-well assay plate in media containing varying concentrations of FGF9 and heparin (Wako). $FGF9^{WT}$ or $FGF9^{Eks}$ were added to each well for a total volume of 200 μl per well. The cells were then incubated at 37°C for 36 hours. 1 μCi of [^{3}H]thymidine was added to each well in 20 μl of media. The cells were harvested after 4 hours by filtration through glass fiber paper and the incorporated [^{3}H]thymidine was counted on a Wallac MicroBeta TriLux scintillation counter (PerkinElmer).

Analytical heparin affinity chromatography

Three mg of purified $FGF9^{WT}$ and $FGF9^{Eks}$ were loaded onto a 1 ml HiTrap heparin HP column (GE healthcare) equilibrated with 25mM ammonium acetate buffer (pH5.5) containing 120 mM NaCl. The bound $FGF9^{WT}$ or $FGF9^{Eks}$ were eluted with a linear gradient of NaCl (120 mM to 2.0 M) in the same buffer.

Surface plasmon resonance analysis of FGF9-heparin interactions

Surface plasmon resonance analysis for measurements of the interactions of $FGF9^{WT}$-heparin and $FGF9^{Eks}$-heparin were performed using a BIAcore 3000 instrument (Biacore AB). In order to immobilize heparin (Wako) on the streptavidin-conjugated sensor chip SA, 100 μg/ml biotinylated heparin in HBS-EP buffer was injected at a flow rate of 10 μl/min and was immobilized to 63 response units (RU). All measurements were carried out at room temperature, and refractive index errors due to bulk solvent effects were corrected by subtracting responses on the non-coated sensor chip for the $FGF9^{WT}$ and $FGF9^{Eks}$ concentrations used. To obtain kinetic data, different concentrations of analytes ($FGF9^{WT}$ and $FGF9^{Eks}$) in HBS-EP were injected over the heparin sensor chip at a flow rate of 20 μl/

min. At the end of each sample injection (120 s), HBS-EP buffer was passed over the sensor surface to monitor the dissociation phase. Following 120 s of dissociation, the sensor surface was regenerated by injection of 5 μl of 1 M NaCl in HBS-EP. Five different analyte concentrations were used to determine the kinetic parameters for each interaction. Kinetic parameters were obtained by global fitting of the sensorgrams to a 1:1 model using BIAevaluation software.

MD simulation

Starting structures of monomeric FGF9^{WT}, dimeric FGF9^{WT}, monomeric FGF9^{WT}-heparin, dimeric FGF9^{WT}-heparin, and those of FGF9^{Eks} for MD simulations were taken from the PDB (PDB ID: 1IHK)14. The structures of monomeric FGF9^{Eks}, dimeric FGF9^{Eks} and heterodimeric FGF9$^{WT/Eks}$ were constructed based on FGF9^{WT} using molecular modeling software MOE (Chemical Computing Group, Inc.). A hexasasaccharide (UAP-SGN-IDU-SGN-IDU-SGN) is used as a heparin oligosaccharide. UAP is 1,4-dideoxy-5-dehydro-O2-sulfo-glucuronic acid, SGN is O6-disulfo-glucosamin and IDU is 1,4-dideoxy-O2-sulfo-glucuronic acid. For monomeric FGF9^{WT}-heparin and dimeric FGF9^{WT}-heparin simulations, heparin oligosaccharide was bound to FGF9^{WT} structures obtained from MD simulations using the molecular docking program GOLD (version 3.0)37. In the docking protocol, the standard default setting of GA parameters was used and GoldScore was used as the scoring function. The structures of monomeric FGF9^{Eks}-heparin and dimeric FGF9^{Eks}-heparin were built in the same manner as FGF9^{WT}-heparin complexes. All the starting structures for MD simulations were surrounded by TIP3P water molecules38 spherically. After energy minimizations, all MD simulations were carried out for 10 ns at 300 K using modified Amber 8.0 (ref. 39) for MDGRAPE3 system40. The Amber ff03 force field41 was adopted, and the simulation time step was set at 1 s. The binding free energies were calculated by the molecular mechanics Poisson-Boltzmann/surface area (MM-PBSA) method42 utilizing the last 2 ns MD trajectories.

Retroviral misexpression

Mouse *Fgf9*^{WT} and *Fgf9*^{Eks} cDNAs were cloned into the RCASBP(A) vector43. The virus solutions were injected into the hind limb bud of chicken embryos at Hamburger-Hamilton (HH) stage 17. The expression of mouse *Fgf9* transcripts and skeletal changes were examined 2 and 5 days after injection, respectively.

Subcutaneous insertion of FGF9^{Eks} beads in mouse fetal skulls

AffiGel-Blue beads (BioRad) soaked in 100 μg/ml FGF9^{WT} or FGF9^{Eks} were implanted onto E15 mouse skulls by *ex utero* surgery as previously described24 Operated heads were collected 24 hours later and *Spp1* transcripts were detected by whole-mount *in situ* hybridization. The area of *Spp1* expression was measured using NIH image software.

Implantation of FGF9^{Eks} beads in mouse forelimb buds

AffiGel-Blue beads that had been soaked in 500 μg/ml FGF9^{WT} or FGF9^{Eks} were implanted into the dorsal and central region of E10.5 *Fgf9*$^{-/-}$ forelimb buds. Limb buds were subsequently cultured for 2 hours on Transwell filters (Costar, Coaning) in serum-free

medium [BGJb, 2 mg/ml BSA, penicillin (50 units/ml), streptomycin (50 μg/ml)], in a humid, 37°C, and 5% CO_2 environment. Explants were fixed in 4% paraformaldehyde and embedded in paraffin. Sections through the equator of the bead were analyzed for exogenous FGF9 using goat anti-human FGF9 antibody (R&D Systems) and a cell and tissue staining kit HRP-AEC system (R&D Systems). The signal area and intensity were analyzed using NIH image software.

IP/Western analysis

cDNA fragments encoding the full length mouse $FGF9^{WT}$ and $FGF9^{Eks}$ proteins were cloned into the p3xFLAG-CMV-14 vector (Sigma-Aldrich) and into the pCMV-Tag3B vector (Stratagene) to allow expression of FGF9 proteins with either C-terminal Myc or 3xFLAG tags. These vectors were transfected into COS7 cells, and 48 h later, culture supernatants were incubated with anti-FLAG M2 affinity beads (Sigma-Aldrich) for 1h at RT and washed three times with PBS, and then subjected to Western blots with anti-FLAG M2 antibody (Sigma-Aldrich) or anti-Myc antibody (Upstate).

Supplementary Material

Refer to Web version on PubMed Central for supplementary material.

ACKNOWLEDGEMENTS

This study was supported in part by the RIKEN Structural Genomics/Proteomics Initiative (RSGI) and the National Project on Protein Structural and Functional Analysis, Ministry of Education, Culture, Sports, Science and Technology of Japan (S. Y.) and NIH grant HD049808 (D. M. O.).

REFERENCES

1. Ornitz DM, Itoh N. Fibroblast growth factors. Genome Biol. 2001; 2(3) REVIEWS3005.
2. Wilkie AOM. Bad bone, absent smell, selfish testes: The pleiotropic consequences of human FGF receptor mutations. Cytokine Growth Factor Rev. 2005; 16:187–203. [PubMed: 15863034]
3. Su N, Du X, Chen L. FGF signaling: its role in bone development and human skeleton diseases. Front. Biosci. 2008; 13:2842–2865. [PubMed: 17981758]
4. Ornitz DM, Marie PJ. FGF signaling pathways in endochondral and intramembranous bone development and human genetic disease. Genes & Dev. 2002; 16:1446–1465. [PubMed: 12080084]
5. Martin GR. The roles of FGFs in the early development of vertebrate limbs. Genes & Dev. 1998; 12:1571–1586. [PubMed: 9620845]
6. Ornitz DM. FGF signaling in the developing endochondral skeleton. Cytokine Growth Factor Rev. 2005; 16:205–213. [PubMed: 15863035]
7. Montero A, et al. Disruption of the fibroblast growth factor-2 gene results in decreased bone mass and bone formation. J. Clin. Invest. 2000; 105:1085–1093. [PubMed: 10772653]
8. Hung IH, Yu K, Lavine KJ, Ornitz DM. FGF9 regulates early hypertrophic chondrocyte differentiation and skeletal vascularization in the developing stylopod. Dev. Biol. 2007; 307:300–313. [PubMed: 17544391]
9. Liu Z, Xu J, Colvin JS, Ornitz DM. Coordination of chondrogenesis and osteogenesis by fibroblast growth factor 18. Genes & Dev. 2002; 16:859–869. [PubMed: 11937493]
10. Ohbayashi N, et al. FGF18 is required for normal cell proliferation and differentiation during osteogenesis and chondrogenesis. Genes & Dev. 2002; 16:870–879. [PubMed: 11937494]

11. Garofalo S, et al. Skeletal dysplasia and defective chondrocyte differentiation by targeted overexpression of fibroblast growth factor 9 in transgenic mice. J. Bone Miner. Res. 1999; 14:1909–1915. [PubMed: 10571691]
12. Ornitz DM. FGFs, heparan sulfate and FGFRs: complex interactions essential for development. BioEssays. 2000; 22:108–112. [PubMed: 10655030]
13. Nybakken K, Perrimon N. Heparan sulfate proteoglycan modulation of developmental signaling in *Drosophila*. Biochim. Biophys. Acta. 2002; 19:280–291. [PubMed: 12417410]
14. Plotnikov AN, et al. Crystal structure of fibroblast growth factor 9 reveals regions implicated in dimerization and autoinhibition. J. Biol. Chem. 2001; 276:4322–4329. [PubMed: 11060292]
15. Hecht HJ, et al. Structure of fibroblast growth factor 9 shows a symmetric dimer with unique receptor- and heparin-binding interfaces. Acta. Crystallogr. D Biol. Crystallogr. 2001; 57:378–384. [PubMed: 11223514]
16. Murakami H, et al. Elbow knee synostosis (Eks): a new mutation on mouse Chromosome 14. Mamm. Genome. 2002; 13:341–344. [PubMed: 12140681]
17. Ornitz DM, et al. Receptor specificity of the fibroblast growth factor family. J. Biol. Chem. 1996; 271:15292–15297. [PubMed: 8663044]
18. Hajihosseini MK, Heath JK. Expression patterns of fibroblast growth factors-18 and -20 in mouse embryos is suggestive of novel roles in calvarial and limb development. Mech. Dev. 2002; 113:79–83. [PubMed: 11900978]
19. Colvin JS, Feldman B, Nadeau JH, Goldfarb M, Ornitz DM. Genomic organization and embryonic expression of the mouse fibroblast growth factor 9 gene. Dev. Dyn. 1999; 216:72–88. [PubMed: 10474167]
20. Wang Q, Green RP, Zhao G, Ornitz DM. Differential regulation of endochondral bone growth and joint development by FGFR1 and FGFR3 tyrosine kinase domains. Development. 2001; 128:3867–3876. [PubMed: 11585811]
21. Eswarakumar VP, Horowitz MC, Locklin R, Morriss-Kay GM, Lonai P. A gain-of-function mutation of *Fgfr2c* demonstrates the roles of this receptor variant in osteogenesis. Proc. Natl. Acad. Sci. 2004; 101:12555–12560. [PubMed: 15316116]
22. Storm EE, Kingsley DM. Joint patterning defects caused by single and double mutations in members of the bone morphogenetic protein (BMP) family. Development. 1996; 122:3969–3979. [PubMed: 9012517]
23. Nalin AM, Greenlee TK, Sandell LJ. Collagen gene expression during development of avian synovial joints: Transient expression of types II and XI collagen genes in the joint capsule. Dev. Dyn. 1995; 203:352–362. [PubMed: 8589432]
24. Iseki S, et al. *Fgfr2* and *osteopontin* domains in the developing skull vault are mutually exclusive and can be altered by locally applied FGF2. Development. 1997; 124:3375–3384. [PubMed: 9310332]
25. Yoshida T, et al. Twist is required for establishment of the mouse coronal suture. J. Anat. 2005; 206:437–444. [PubMed: 15857364]
26. Flaumenhaft R, Moscatelli D, Rifkin DB. Heparin and heparan sulfate increase the radius of diffusion and action of basic fibroblast growth factor. J. Cell Biol. 1990; 111:1651–1659. [PubMed: 2170425]
27. Woo HJ, Roux B. Calculation of absolute protein-ligand binding free energy from computer simulations. Proc. Natl. Acad. Sci. 2005; 102:6825–6830. [PubMed: 15867154]
28. Schlessinger J, et al. Crystal structure of a ternary FGF-FGFR-heparin complex reveals a dual role for heparin in FGFR binding and dimerization. Mol. Cell. 2000; 6:743–750. [PubMed: 11030354]
29. Dowd CJ, Cooney CL, Nugent MA. Heparan sulfate mediates bFGF transport through basement membrane by diffusion with rapid reversible binding. J. Biol. Chem. 1999; 274:5236–5244. [PubMed: 9988774]
30. Johnson D, Iseki S, Wilkie AOM, Morriss-Kay GM. Expression patterns of Twist and *Fgfr1, −2* and *−3* in the developing mouse coronal suture suggest a key role for Twist in suture initiation and biogenesis. Mech. Dev. 2000; 91:341–345. [PubMed: 10704861]
31. Tsang M, Dawid IB. Promotion and attenuation of FGF signaling through the Ras–MAPK pathway. Sci. STKE 2004. 2004; 228:pe17.

32. Mohammadi M, Olsen SK, Ibrahimi OA. Structural basis for fibroblast growth factor receptor activation. Cytokine Growth Factor Rev. 2005; 16:107–137. [PubMed: 15863029]
33. Ornitz DM, et al. Heparin is required for cell-free Binding of Basic Fibroblast Growth Factor to a Soluble Receptor and for mitogenesis in whole cells. Mol. Cell Biol. 1992; 12:240–247. [PubMed: 1309590]
34. Venkataraman G, Shriver Z, Davis JC, Sasisekharan R. Fibroblast growth factors 1 and 2 are distinct in oligomerization in the presence of heparin-like glycosaminoglycans. Proc. Natl. Acad. Sci. 1999; 96:1892–1897. [PubMed: 10051565]
35. Kessel M, Gruss P. Murine developmental control genes. Science. 1990; 249:374–379. [PubMed: 1974085]
36. Kessel M, Gruss P. Homeotic transformations of murine vertebrae and concomitant alteration of Hox codes induced by retinoic acid. Cell. 1991; 67:89–104. [PubMed: 1680565]
37. Verdonk ML, Cole JC, Hartshorn MJ, Murray CW, Taylor RD. Improved protein-ligand docking using GOLD. Proteins. 2003; 52:609–623. [PubMed: 12910460]
38. Jorgensen WL, Chandrasekhar J, Madura JD, Impey RW, Klein ML. Comparison of simple potential functions for simulating liquid water. J. Chem. Phys. 1983; 79:926–935.
39. Case, DA., et al. AMBER 8. San Francisco: University of California; 2004.
40. Narumi T, et al. A 185 Tflops simulation of amyloid-forming peptides from Yeast Prion Sup35 with the special-purpose computer System MD-GRAPE3. Supercomputing. 2006
41. Duan Y, et al. A point-charge force field for molecular mechanics simulations of proteins based on condensed-phase quantum mechanical calculations. J. Comput. Chem. 2003; 24:1999–2012. [PubMed: 14531054]
42. Srinivasan J, Miller J, Kollma PA, Case DA. Continuum solvent studies of the stability of RNA hairpin loops and helices. J. Biomol. Struct. Dyn. 1998; 16:671–682. [PubMed: 10052623]
43. Hughes SH, Greenhouse JJ, Petropoulos CJ, Sutrave P. Adaptor plasmids simplify the insertion of foreign DNA into helper-independent retroviral vectors. J. Virol. 1987; 61:3004–3012. [PubMed: 3041020]

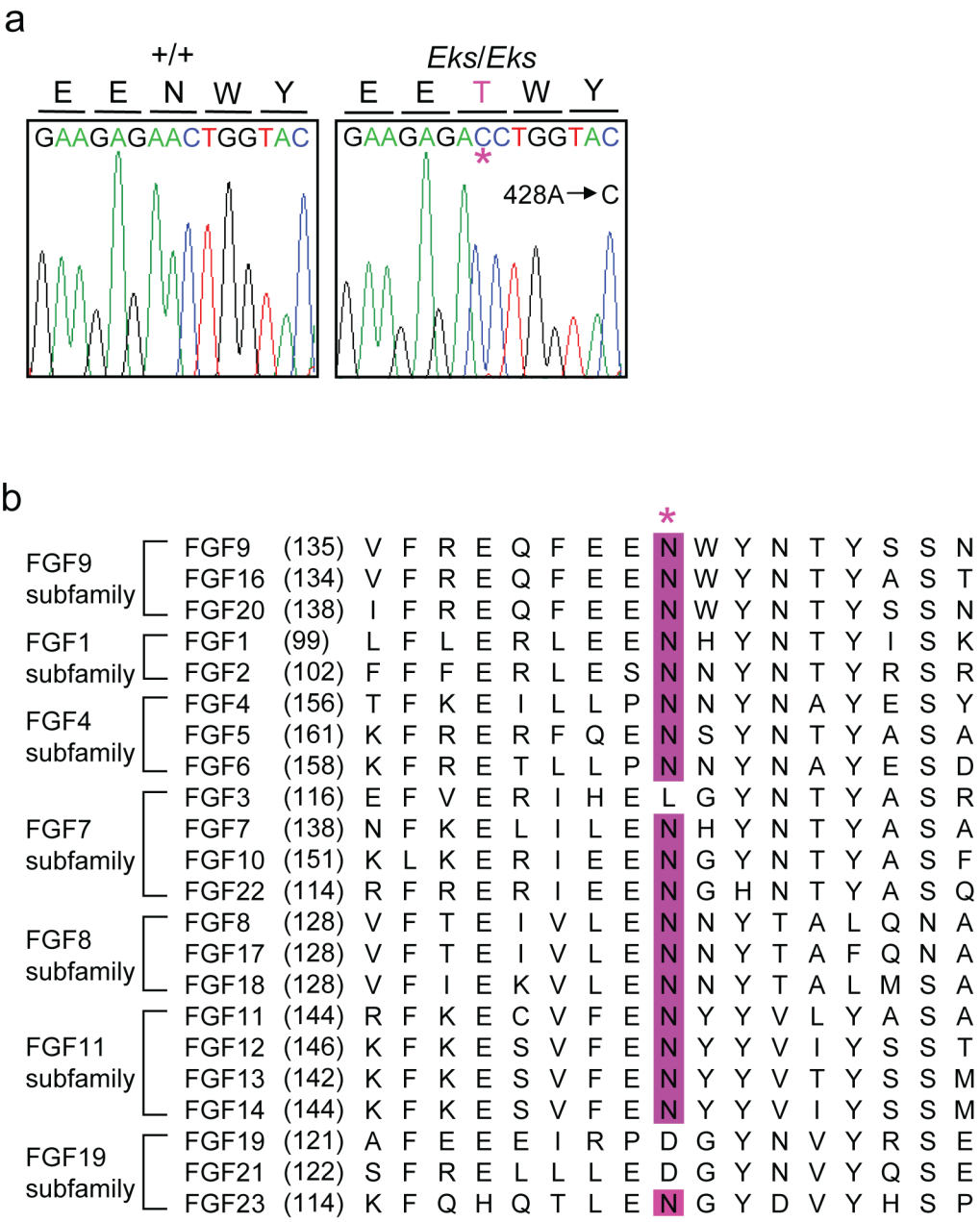

Figure 1.

Missense mutation in the *Fgf9* gene of *Eks* mice. (**a**) Nucleotide sequence of the *Fgf9* cDNA derived from +/+ and *Eks/Eks* mice. *Eks* mutants have an A to C substitution at position 428, which results in the replacement of Asn143 with Thr. The *Eks* missense mutation is indicated by the asterisk and the corresponding amino acid is shown in purple. (**b**) Structure-based sequence alignment of human FGFs. The amino acid sequence surrounding the N143T mutation in FGF9^{Eks} and that of its corresponding domain in other human FGF family proteins are aligned based on sequence identity. The Asn143 residue in FGF9 is

highly conserved among most FGF proteins (purple box). The asterisk denotes the site of *Eks* mutation.

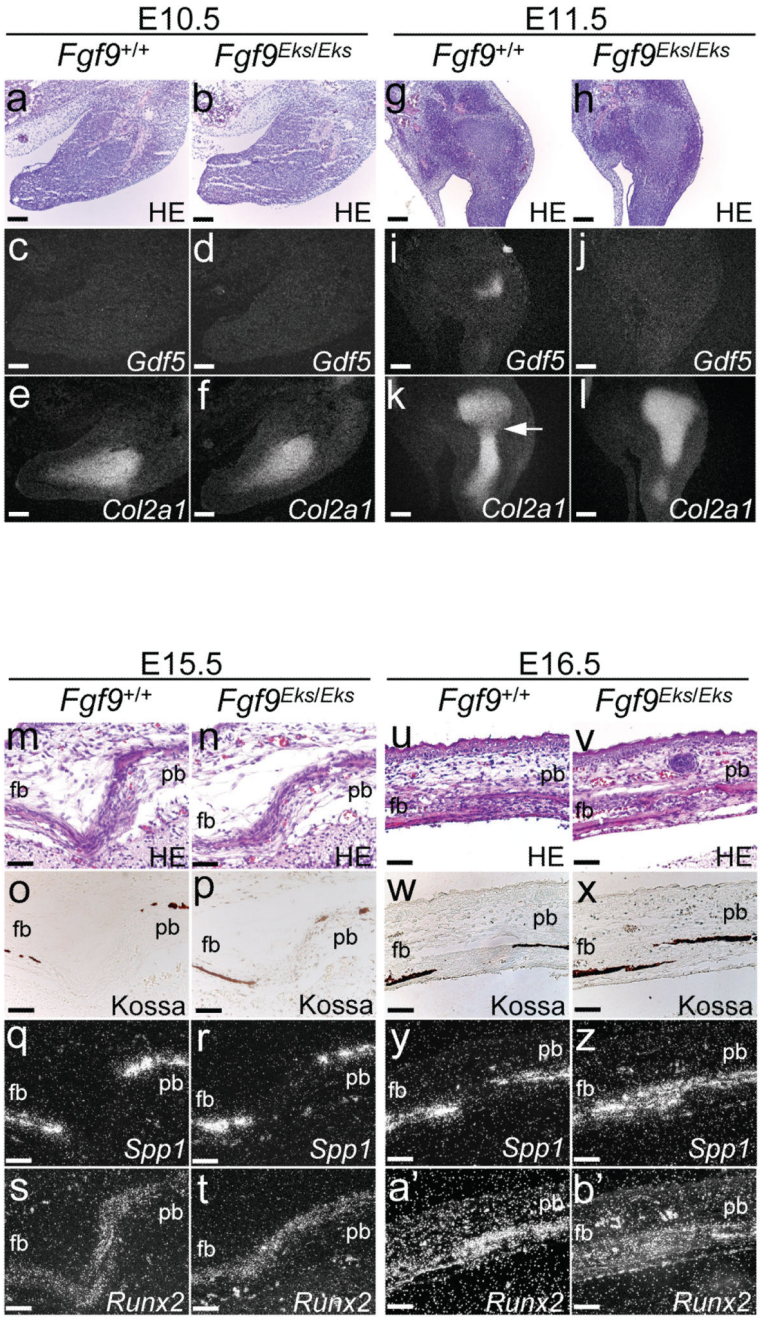

Figure 2.

Fgf9$^{Eks/Eks}$ mice phenocopy *Fgfr*s gain-of-function mutants. (**a–l**) Defects in early specification of prospective elbow joints in *Fgf9*$^{Eks/Eks}$ embryos. Hematoxylin and eosin staining (**a, b, g, h**) and *in situ* detection of *Gdf5* (**c, d, i, j**) and *Col2a1* (**e, f, k, l**) in the forelimb buds of *Fgf9*$^{+/+}$ and *Fgf9*$^{Eks/Eks}$ embryos at E10.5 and E11.5. In *Fgf9*$^{+/+}$ embryos there was *Gdf5* expression at the prospective elbow joint (**i**), which was demarcated as the gap of *Col2a1* expression (**k**, arrow), at E11.5. In *Fgf9*$^{Eks/Eks}$ embryos there was not *Gdf5* expression at the prospective elbow joint (**j**). Scale bars, 100 μm. (**m–b'**) Ectopic

osteogenesis at the coronal sutures in *Fgf9*$^{Eks/Eks}$ fetuses. Hematoxylin and eosin staining (**m, n, u, v**) and von Kossa staining (**o, p, w, x**) and *in situ* detection of *Spp1* (**q, r, y, z**) and *Runx2* (**s, t, a', b'**) in the coronal suture of *Fgf9*$^{+/+}$ and *Fgf9*$^{Eks/Eks}$ fetuses at E15.5 and E16.5. Note the ectopic ossification in the suture of *Fgf9*$^{Eks/Eks}$ at E16.5 (**v, x, z, b'**). fb, frontal bone; pb, parietal bone. Scale bars, 100 μm.

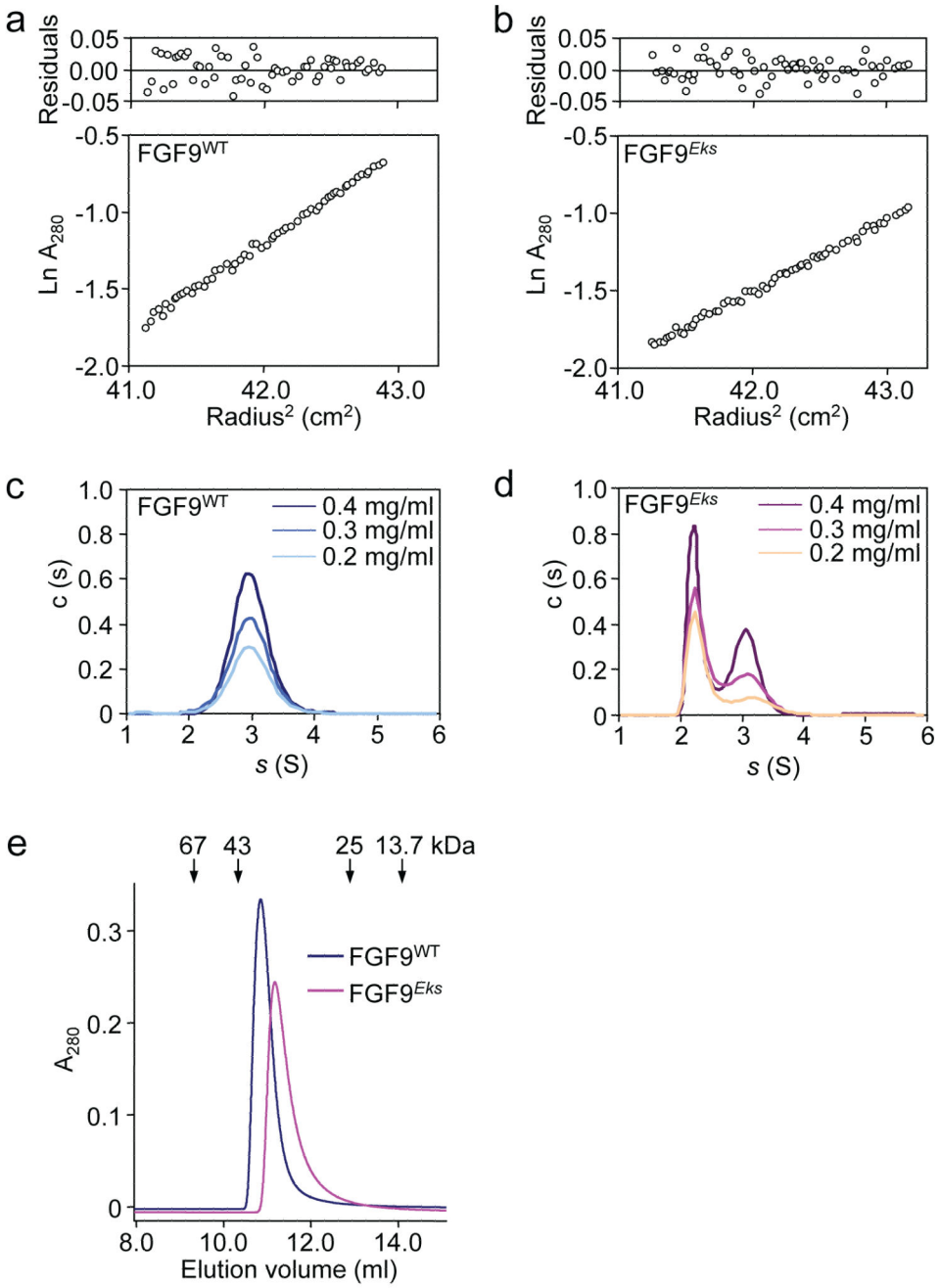

Figure 3.

The *Eks* mutation affects dimerization of FGF9. (**a, b**) Sedimentation equilibrium analysis of FGF9^{WT} and FGF9^{Eks}. Ln A_{280nm} versus radius^2 during sedimentation equilibrium at 16,000 rpm at 20°C is indicated using 0.4 mg/ml of FGF9^{WT} (**a**) and FGF9^{Eks} (**b**). The residuals are shown in the upper panels. (**c, d**) Sedimentation velocity analysis of FGF9^{WT} and FGF9^{Eks}. The sedimentation coefficient distribution for FGF9^{WT} (**c**) and FGF9^{Eks} (**d**) at the concentrations of 0.2, 0.3 and 0.4 mg/ml are shown. (**e**) Analytical gel filtration chromatography of FGF9^{WT} and FGF9^{Eks}. FGF9^{WT} or FGF9^{Eks} applied separately to

Superdex 75 10/300 GL columns. Eluted $FGF9^{WT}$ and $FGF9^{Eks}$ were identified by absorbance at 280 nm. Arrows indicate the position of the size standards: 67 kDa, albumin; 43 kDa, ovalbumin; 25 kDa, chymotrypsinogen; 13.7 kDa, ribonuclease A.

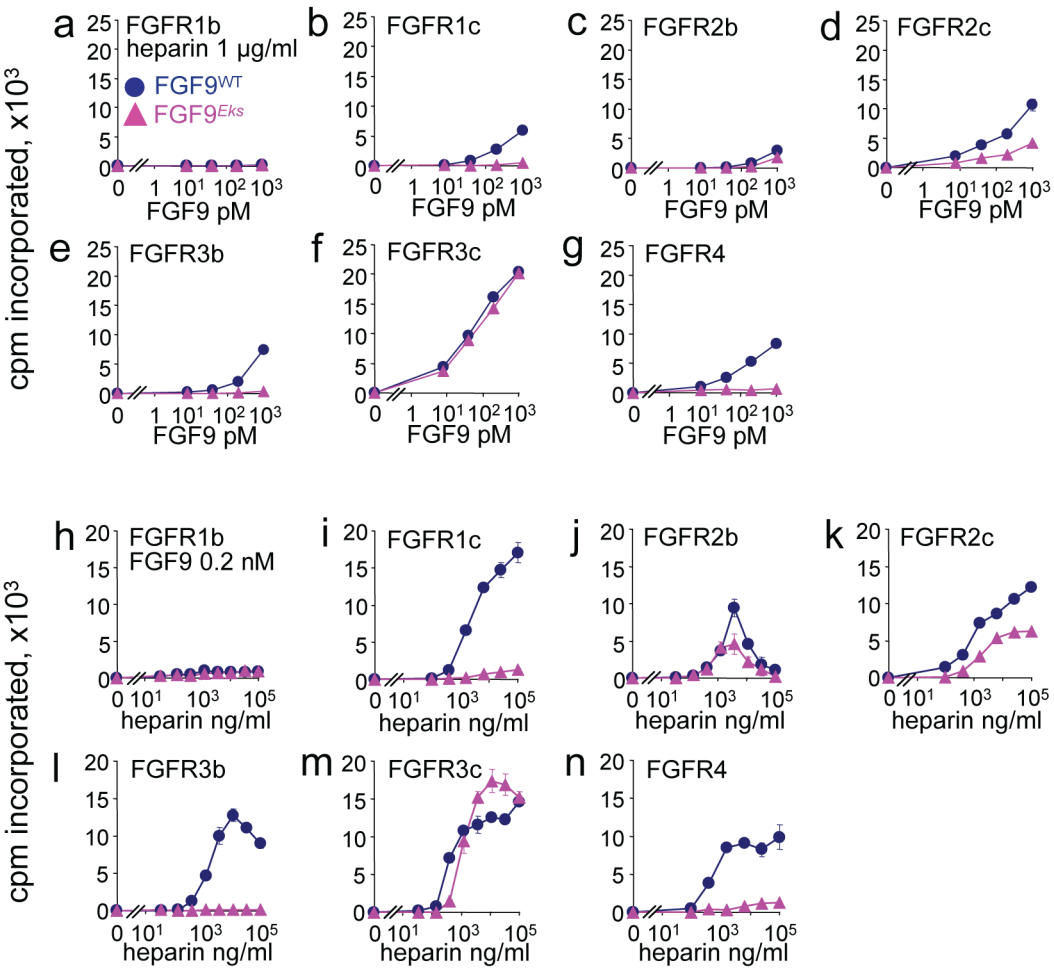

Figure 4.

The *Eks* mutation affects the mitogenic activity of FGF9. (**a–g**) Dose dependent changes in mitogenic activity of $FGF9^{WT}$ and $FGF9^{Eks}$. BaF3 cells expressing exogenous FGFR1b, 1c, 2b, 2c, 3b, 3c or 4 were treated with increasing concentrations of $FGF9^{WT}$ or $FGF9^{Eks}$ in the presence of 1 µg/ml heparin. Cell proliferation was determined by [^{3}H]thymidine incorporation after 36 hours in culture. (**h–n**) Heparin-dependent changes in mitogenic activity of $FGF9^{WT}$ and $FGF9^{Eks}$. BaF3 cells expressing the respective FGFR were treated with increasing concentrations of heparin in the presence of 0.2 nM $FGF9^{WT}$ or $FGF9^{Eks}$. Cell proliferation was determined as above. Data are represented as mean ± s.e.m. of triplicate assays. These results are representative of at least two independent experiments.

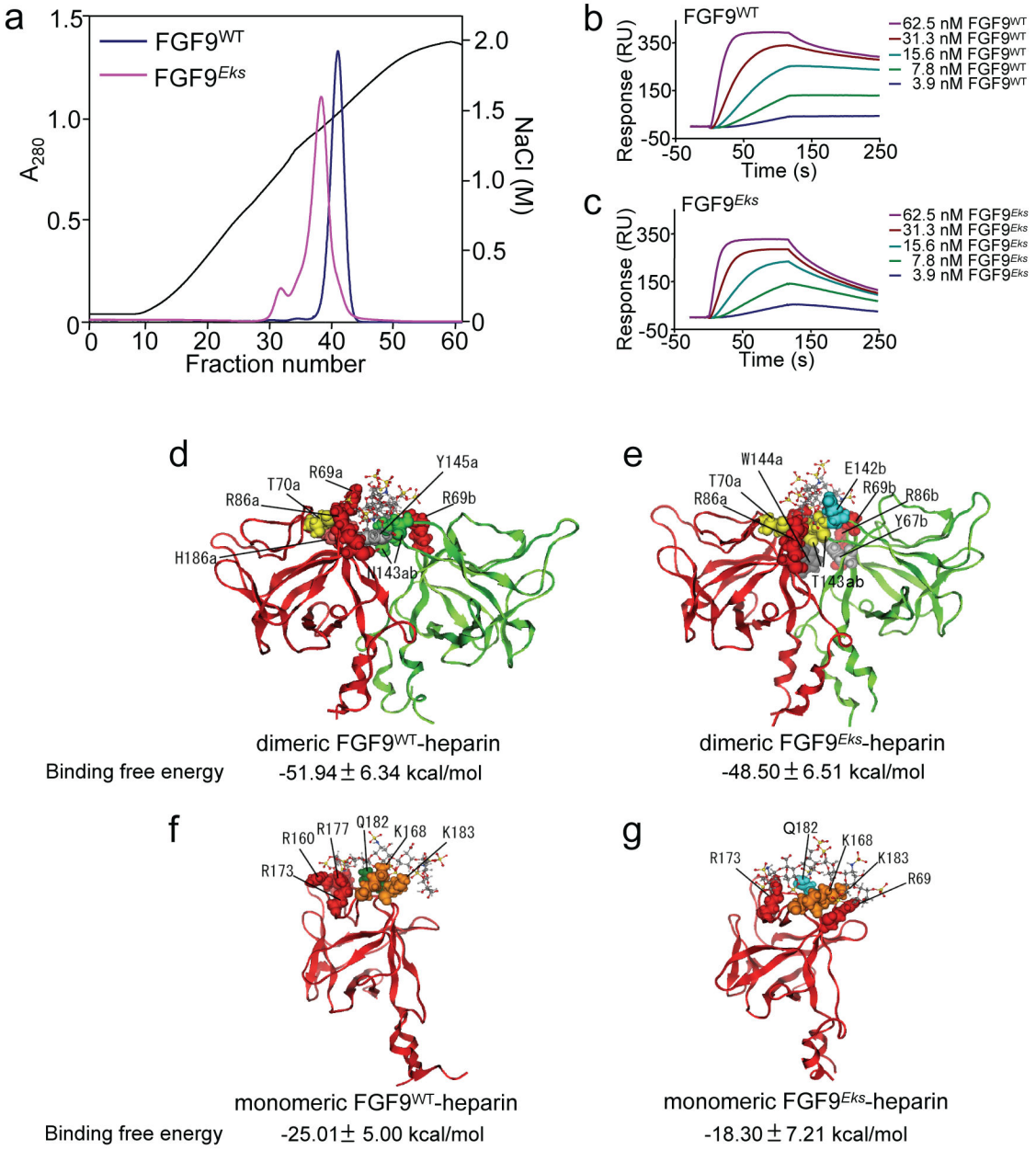

Figure 5.

The *Eks* mutation reduces FGF9 affinity for heparin by impairing its dimerization. (**a**) Chromatographic analysis of the affinities of FGF9^{WT} and FGF9^{Eks} for heparin. FGF9^{WT} or FGF9^{Eks} were loaded onto a heparin-conjugated agarose column and eluted with a linear gradient of NaCl from 120 mM to 2.0 M (black line). Elution profiles of FGF9^{WT} and FGF9^{Eks} were determined by monitoring absorbance at 280 nm. (**b, c**) Surface plasmon resonance analysis of the affinities of FGF9^{WT} and FGF9^{Eks} for heparin. Sensorgrams indicating the interaction of FGF9^{WT} (**b**) and FGF9^{Eks} (**c**) with immobilized heparin were determined at different concentrations. The biosensor chip response is indicated on the y-axis (RU) as a function of time (x-axis) at room temperature. (**d–g**) The most probable

solution structures of dimeric FGF9^{WT}-heparin (**d**), dimeric FGF9^{Eks}-heparin (**e**), monomeric FGF9^{WT}-heparin (**f**) and monomeric FGF9^{Eks}-heparin (**g**) complexes deduced by MD simulations. Heparin and protein residues that form important hydrogen bonds are drawn in ball and stick and space-filling modes. The single-letter amino acid code, residue number and chain code are indicated for each of these residues. Computed binding free energy of each complex is shown under the respective illustrated structure. Data are represented as mean ± s.d. of energies obtained from 200 MD snapshots in respective MD trajectory.

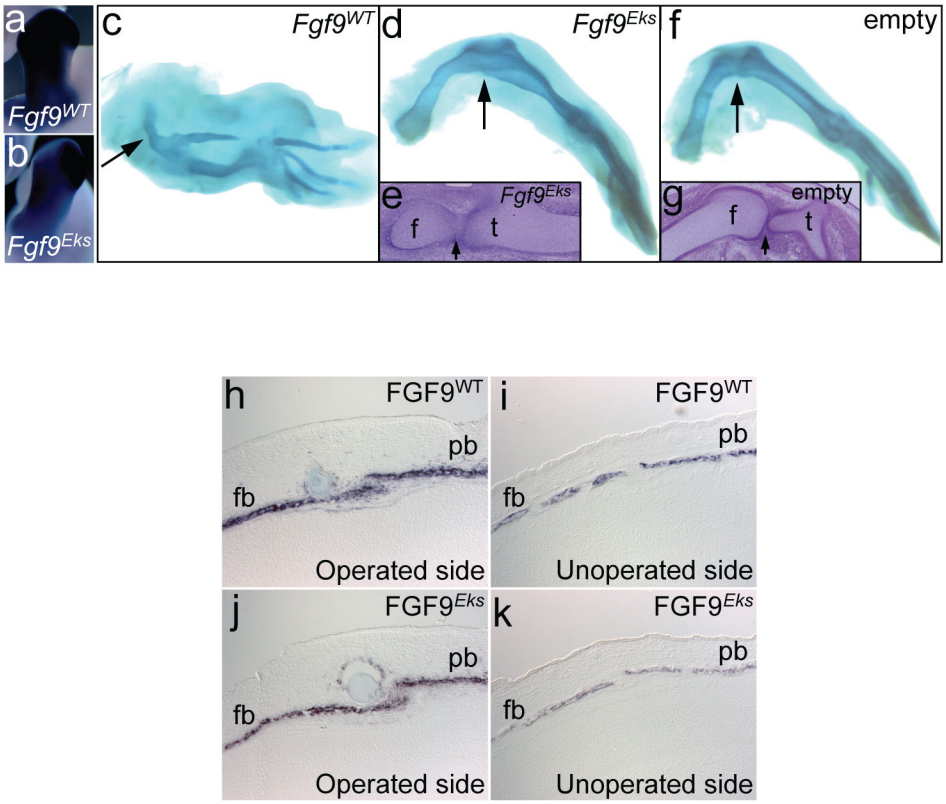

Figure 6.

FGF9^{Eks} can inhibit joint and suture development as well as FGF9^{WT}. (**a–g**) Inhibition of knee joint development induced by ectopic expression of *Fgf9*^{Eks} as well as *Fgf9*^{WT}. Hindlimb buds of HH stage 17 chickens were infected with RCAS-*Fgf9*^{WT}, RCAS-*Fgf9*^{Eks}, or empty RCAS virus. (**a, b**) *Fgf9* expression was examined by *in situ* hybridization 2 days after infection. (**c–g**) Respective knee joints (arrows) were examined by Alcian blue staining (**c, d, f**) and hematoxylin and eosin staining of sections through the knee joint (**e, g**) 5 days after infection. f, femur; t, tibia. (**h–k**) Inhibition of coronal suture development by the ectopic presence of FGF9^{Eks} well as FGF9^{WT}. FGF9^{WT} or FGF9^{Eks} beads were implanted onto the coronal suture at E15 mice and the *Spp1* expression was examined by *in situ* hybridization 24 hours after implantation. On the operated sides with FGF9^{WT} (**h**) and FGF9^{Eks} (**j**) bead implants, there was overlap of *Spp1* expression in the frontal and parietal bones, which was not seen on the unoperated sides (**i, k**). fb, frontal bone; pb, parietal bone.

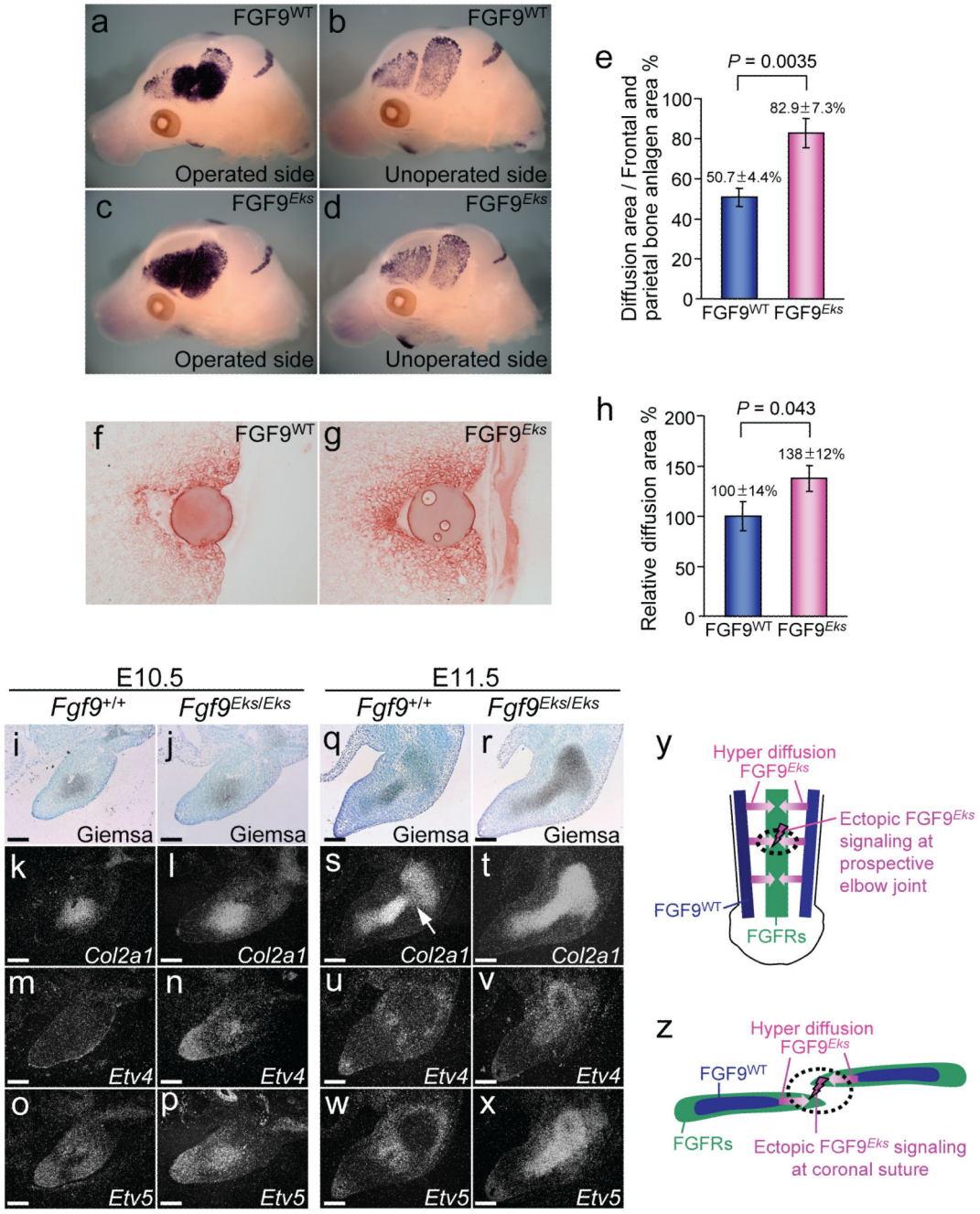

Figure 7.

Ectopic FGF9^{Eks} signaling due to its hyper diffusibility. (**a–e**) Increased diffusibility of FGF9^{Eks} in the skull bone anlagen. FGF9^{WT} or FGF9^{Eks} beads were implanted onto the coronal suture at E15 mice and *Spp1* expression was examined by whole-mount *in situ* hybridization 24 hours after implantation. On the operated sides with FGF9^{WT} (**a**) and FGF9^{Eks} (**c**) bead implants, we observed well-defined intense signals in the frontal and parietal bone anlagen around the implants, which were not seen on the unoperated side (**b, d**). This domain with intense *Spp1* signals reflects diffusibility of exogenous FGF9 proteins.

We therefore compared diffusibility of $FGF9^{WT}$ and $FGF9^{Eks}$ based on the induced expression domain of *Spp1* (**e**). The diffusion areas (%) in the frontal and parietal bone anlagen area were estimated from the area ratio of the intense *Spp1* expression against the frontal and parietal bone anlagen. Data are represented as mean ± s.e.m. of six operations. $FGF9^{Eks}$ is more diffusible than $FGF9^{WT}$. Significance was determined by two-tailed Student's *t*-test. (**f–h**) Increased diffusibility of $FGF9^{Eks}$ in the forelimb bud. $FGF9^{WT}$ or $FGF9^{Eks}$ beads were implanted into forelimb buds of $Fgf9^{-/-}$ embryos of E10.5 mice. Diffusion of exogenous $FGF9^{WT}$ (**f**) and $FGF9^{Eks}$ (**g**) after 2 hours was immunodetected using a FGF9 antibody. (**h**) The diffusion area of $FGF9^{Eks}$ and $FGF9^{WT}$ was measured at the level of the equator of the beads. Data are represented as mean ($FGF9^{WT}$ =100%) ± s.e.m. of four ($FGF9^{WT}$) or five ($FGF9^{Eks}$) operations. $FGF9^{Eks}$ is also more diffusible than $FGF9^{WT}$ in limb buds. Significance was determined by one-tailed Student's *t*-test. (**i–x**) The downstream target genes of FGF signaling, *Etv4* and *Etv5*, are expressed ectopically in the prospective elbow joint in $Fgf9^{Eks/Eks}$ mice. Counterstaining with Giemsa (**i, j, q, r**) and *in situ* detection of *Col2a1* (**k, l, s, t**), *Etv4* (**m, n, u, v**) and *Etv5* (**o, p, w, x**) in the forelimb buds of $Fgf9^{+/+}$ and $Fgf9^{Eks/Eks}$ embryos at E10.5 and E11.5. There was ectopic expression of *Etv4* (**n, v**) and *Etv5* (**p, x**), in the cartilaginous condensation including the prospective elbow joint position, which was demarcated as the gap of *Col2a1* expression (**s**, arrow), in $Fgf9^{Eks/Eks}$, which were not seen in $Fgf9^{+/+}$ mice (**m, o, u, w**). Scale bars, 100 μm. (**y**) A model for the pathogenic mechanism underlying elbow joint synosotsis in $Fgf9^{Eks/Eks}$ mice. In $Fgf9^{Eks/Eks}$ mice, ectopic FGF9 signaling due to hyper-diffusion of $FGF9^{Eks}$ at the prospective elbow joint may inhibit the initiation of joint development. (**z**) A model for the pathogenic mechanism underlying premature fusion of the coronal suture in $Fgf9^{Eks/Eks}$ mice. In $Fgf9^{Eks/Eks}$ mice, ectopic FGF9 signaling due to hyper-diffusion of $FGF9^{Eks}$ at the coronal suture may promote ectopic osteogenesis and subsequently induce premature fusion of the suture.

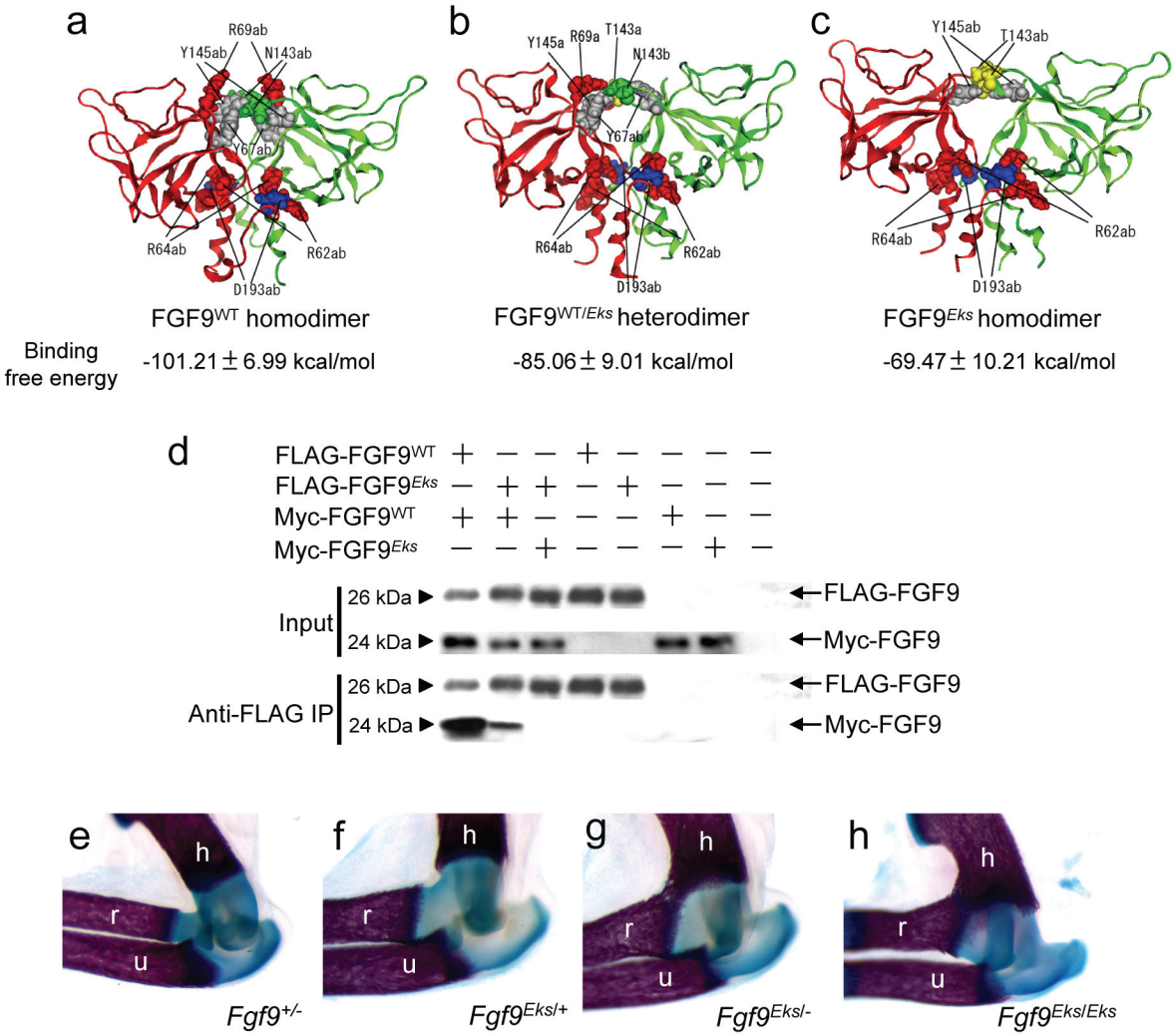

Figure 8.

FGF9^{WT} modulates FGF9^{Eks} action by forming FGF9^{WT}/FGF9^{Eks} heterodimers. (**a–c**) Proposed solution structures for FGF9^{WT} homodimer (**a**), FGF9$^{WT/Eks}$ heterodimer (**b**) and FGF9^{Eks} homodimer (**c**). Amino acid residues contributing to hydrogen bond formation involved in dimerization are drawn in ball and stick and space-filling modes. The single-letter amino acid code, residue number and chain code are indicated for each of these residues. Computed binding free energy of each dimer is shown under the respective illustrated structure. Data are represented as mean ± s.d. of energies obtained from 200 MD snapshots in respective MD trajectory. (**d**) FGF9^{WT} is capable of forming dimers with FGF9^{Eks}. The expression of FGF9^{WT} homodimers, FGF9$^{WT/Eks}$ heterodimers and FGF9^{Eks} homodimers was analyzed using IP/Western blots. The expression vectors for FLAG- or Myc-tagged FGF9^{WT} and FGF9^{Eks} were transfected into COS7 cells and culture supernatants were subjected to IP/Western analysis. (**e–h**) Less severe elbow joint synostosis in *Fgf9*$^{Eks/+}$ than *Fgf9*$^{Eks/−}$. Forelimbs from *Fgf9*$^{+/−}$, *Fgf9*$^{Eks/+}$, *Fgf9*$^{Eks/−}$ and *Fgf9*$^{Eks/Eks}$ embryos at E17.5 were stained with Alcian blue and Alizarin red. Synostotic change is

restricted to the cartilaginous component in *Fgf9*$^{Eks/+}$ embryos, whereas it is extended to the bony component in *Fgf9*$^{Eks/-}$, and *Fgf9*$^{Eks/Eks}$ embryos. h, humerus; r, radius; u, ulna.